The implication of PMMA molecular weight on compatibility of SAN/PMMA blends containing GO-g-PMMA hybrid compatibilizers

The implication of PMMA molecular weight on compatibility of SAN/ PMMA blends containing GO-g-PMMA hybrid compatibilizers

Szymon Kozlowski[a], Magdalena Lipińska[a], Miroslav Slouf[b], Miroslav Mrlik[c], Christopher M. Plummer[d], Marketa Ilcikova[c,e,f], Josef Osička[c], Joanna Pietrasik[a,*]

[a]Lodz University of Technology, Department of Chemistry, Institute of Polymer and Dye Technology, Stefanowskiego 16, 90-537 Lodz, Poland

[b]Czech Academy of Sciences, Institute of Macromolecular Chemistry, Heyrovskeho nam. 2, Praha 16206, Czech Republic

[c]Tomas Bata University in Zlin, Centre of Polymer Systems, tr. Tomase Bati 5678, Zlin 76001, Czech Republic

[d]Lodz University of Technology, International Center for Research on Innovative Biobased Materials (ICRI-BioM)—International Research Agenda, Zeromskiego 116, Lodz 90-924, Poland

[e]Slovak Academy of Sciences, Polymer Institute, Dubravska cesta 9, 845 41 Bratislava, Slovakia

[f]Deparment of Physics and Materials Engineering, Faculty of Technology, Tomas Bata University, Vavreckova 5669, Zlin 76001, Czech Republic

[*]Corresponding author. E-mail address: joanna.pietrasik@p.lodz.pl (J. Pietrasik).

ABSTRACT

The molecular weight of a polymer is one of the most important factors defining material properties and performance. Within the current study, poly(styrene-co-acrylonitrile)/poly(methyl methacrylate) ($SAN/PMMA$) blends containing hybrid particles of graphene oxide-g-poly(methyl methacrylate) ($GO-g-PMMA$) were designed so that the molecular weight of the $PMMA$ chains tethered on the GO particles was correlated with the molecular weight of the $PMMA$ matrix. Hybrid particles were prepared using surface-initiated atom transfer radical polymerization ($ATRP$). The number average molecular weight of the matrix $PMMA$ was M_n = 20,100 or 130,900 g/mol, while in the case of hybrids it was M_n = 5600, 27,300 or 191,600 g/mol. Two blend compositions were investigated: $SAN/PMMA$ = 70/30 and 90/10 wt/wt, and the content of $GO-g-PMMA$ was 1 wt%. Based on rheological studies it was demonstrated that higher molecular weights of the matrix $PMMA$ promoted the compatibility of $SAN/PMMA$ due to the similar viscosity of both blend components. Furthermore, the length of the PMMA chains grafted to the GO influenced the viscoelastic response of the material, resulting in different relaxation behavior as confirmed by mean relaxation times calculated from Cole-Cole plots. In addition, the effect of neat GO and $GO-g-PMMA$ particles on the blend morphology and size distribution of $PMMA$ droplets was discussed based on rheology and TEM analyses.

Keywords: SAN/PMMA blends, polymer brushes, graphene oxide, rheological properties, blend compatibilization

1. Introduction

Polymer blends have gained significant attention because they are an inexpensive and simple way to produce new materials with novel properties [**1-3**]. For example, combining two different polymers is an effective way to improve a polymer's mechanical properties, miscibility, and thermal stability while maintaining the original properties of the parent homopolymers [**1,4,5**]. The performance of polymer blends is strongly influenced by the blend's composition, processing condition, and the presence of additives that play a key role as blend compatibilizers, fillers, or stabilizers.

The majority of polymers show immiscibility with each other, exhibiting phase separation due to low mixing entropy and high interfacial tension [**6**]. In the case of miscible blends, miscibility occurs on a molecular level and the degree of modification to the material properties depends upon the miscibility of the components which are contained within the polymer blend [**7,8**]. Miscibility is a complex phenomenon resulting from many factors [**7**]. One of the factors that determines miscibility is the exothermic heat of mixing, which is influenced by dipolar, hydrogen bonding, and charge transfer interactions [**8,9**]. Miscibility can also occur due to intramolecular repulsive forces in the components of the polymer blend [**2,7,8**]. A good example of a miscible system is the poly(styrene-co-acrylonitrile)/poly (methyl methacrylate) ($SAN/PMMA$) blend. To achieve miscibility, the acrylonitrile content in SAN must be in the range of 9-33 wt% [**2,10**]. Kumaraswamy et al. [**8**] claimed that an important factor for obtaining miscibility is also the hydrodynamic parameter a which is a measure of excess friction between the polymer chains of the constituent polymers. In a miscible system, parameter a has a higher value because chain entanglements generate additional friction. The processing window in which the a value has high values is the concentration of $PMMA$ in the range of 10-30 wt%.

The addition of nanoparticles to a polymer system draws a lot of attention because it is an efficient way to tune the final properties of a materials. For example, the addition of silica, carbon nanotubes or graphene oxide, etc., can result in changes to mechanical, electrical, optical, and permeability properties of the resulting composite [**11,12**]. In addition to improving the final properties, it is also possible to use nanoparticles as blend compatibilizers to slow phase separation of the system and control the morphology of immiscible polymer blends [**13, 14**]. To obtain a good compatibilization efficiency, nanoparticles should have a good distribution in the polymer mixture or be selectively localized in one of the phases of the polymer mixture [**14**]. Surface modification of nanoparticles with polymers with similar structures to the parent polymers is a promising way to obtain compatibilizers which will also improve the desired properties [**15,16**].

The use of modified GO is an interesting way to compatibilize polymer blends. The presence of oxygen-containing functional groups allows for the chemical modification of GO particles [**17**]. Surface modification can be performed using small-molecule compounds or polymers. Different grafting approaches can be used to attach polymer chains to the surface of nanoparticles, including 'grafting to', 'grafting from', and 'grafting through' methods [**18**]. The combination of 'grafting from' with reversible deactivation radical polymerization ($RDRP$) is often applied [**18,19**]. Surface-initiated atom transfer polymerization ($SI-ATRP$) is a common approach for the synthesis of well-defined polymer brushes on the surface of a substrate as it maintains good control over polymer molecular weight, dispersity, and end-group functionality [**19,20**].

Nanofiller modified in this way could localize at the interface of the blend and as a result reduce the surface tension between components [**21,22**]. However, it can be also selectively localized in one of the polymer phases, due to preferential wettability [**22**] resulting from the varied length of the polymer chain that is grafted onto the nanofiller surface. Nanoparticles with a grafted polymer similar to the matrix and with a gyration radius of the polymer chains lower than the gyration radius of the matrix are expected to be expulsed from the matrix [**23**]. However, as was demonstrated in our previous studies [**2**], graphene oxide particles with tethered short and dense polystyrene brushes ($GO-g-PS$) suppressed the phase separation of miscible $SAN/PMMA$ blends due to the unusual and specific interactions of $GO-g-PS$ with the $PMMA$ phase. In this work, graphene oxide was modified with $PMMA$ chains (6000 g/mol, 27,000 g/mol, and 190,000 g/mol) and used as a nanofiller in $SAN/PMMA$ blends with a ratio of 70/30 and 90/10. The blend composition was selected to be on the edge of the miscibility window [**8**] while the molecular weight of the $PMMA$ chains grafted onto the GO surface was varied to observe the changes in the rheological behavior of the blends and the impact of this parameter on blend com-patibilization. To the best of our knowledge, a comprehensive investigation regarding the dependence of the molecular weight of the $PMMA$ in the polymer matrix and the $PMMA$ grafted to the particle surface in relation to rheological properties has not been reported.

2. Experimental

2.1. Materials

Reagents and chemicals including, triethylamine ($\geq$ 99.5%), 2-bromo-2-methylpropionyl bromide ($BiBB$, 98%), N,N,N',N",N"-pentam-ethyldiethylenetriamine ($PMDETA$, 99%), ethyl a-bromoisobutyrate ($EBiB$, 98%), 1,1,4,7,10,10-hexamethyltriethylenetetramine ($HMTETA$, 97%), fuming nitric acid (100%), potassium chlorate, hydrochloric acid and anisole ($ReagentPlus$®, 99%), copper (I) bromide ($CuBr$, ≥99.999%), copper (II) bromide ($CuBr_2$, ≥99.999%) and monomer methyl methacrylate (MMA, 99%) were purchased from Sigma-Aldrich. All solvents were purchased from Pure $POCH$ and used without further purification. MMA monomer was purified before use by passing through a column filled with basic alumina. The polymer matrix $KOSTIL$ B366 poly(styrene-co-acrylonitrile) (SAN, acrylonitrile content 20.3%, M_n = 223,300 g/mol, **D** = 1.37) was received from Versalis (IT) and used as received.

2.2. Synthesis of linear polymers and hybrid particles

2.2.1. Synthesis of linear (matrix) poly(methyl methacrylate) (PMMA)

(12.1 mg, 0.054 mmol) were added into a Schlenk flask (100 mL) containing a magnetic stirring bar. The flask was evacuated and backfilled with argon and the procedure was repeated three times. The anisole (12.0 mL) and monomer (12.0 mL, 0.11 mol) were purged with argon and then added to the Schlenk flask under argon flow. Next, the ligand $HMTETA$ (98.7 μL, 0.36 mmol) in 1 mL of anisole and $EBiB$ (94.1 μL, 0.36 mmol) in 1 mL of anisole were taken from purged stock solutions and added to the reaction flask. The reaction was started by immersion of the flask into an oil bath preheated to 70 °C. The obtained polymer solution was diluted with acetone and passed through a column filled with neutral alumina. Excess acetone was removed by rotary evaporator (50 °C, 500 mbar) and the polymer was precipitated in methanol. The final product was dried in a vacuum oven at 40 °C and 10 mbar for 2 days.

2.2.2. Preparation of graphene oxide (GO)

Graphene oxide was prepared according to a modified Brodie method [**24**]. Briefly, fuming nitric acid (100%, 125 mL) was added slowly to a reaction flask containing a magnetic stirring bar. The mixture was subsequently cooled to approximately 0 ° C in a water/ice bath and graphite was loaded (10 g). The mixture was stirred to obtain a homogenous dispersion. While keeping the reaction at 0 °C, potassium chlorate (50 g) was slowly added to the dispersion. Upon complete dissolution of potassium chlorate, the reaction flask was loosely capped to allow the escape of the evolved gas, and the mixture was stirred for 20 h at 40 °C. After that, the mixture was mixed with 1 L of distilled water and centrifuged, and this was performed three times. Then the GO was dispersed in 5% HCl solution (3 L) to remove metal ions followed by centrifugation. Finally, it was washed with distilled water and then dried in a freeze drier.

2.2.3. Graphene oxide modification with ATRP initiator (GO-Br)

The 2-bromo-2-methylpropionyl bromide ($BiBB$) initiator was introduced onto the GO surface according to a procedure described in the literature [**25**]. Briefly, the GO powder (2 g) was introduced into a three-neck round-bottom flask (250 mL), then the flask was evacuated and backfilled with argon several times. Anhydrous THF (60 mL) was added to a flask with GO under argon flow. The mixture was sonicated shortly in an ultrasound bath to disperse the particles in the solvent. Then triethylamine (12 mL, 86 mmol) was added into the reaction flask under argon flow. The mixture was cooled to — 5 °C in an ice/water bath and $BiBB$ (7 mL, 57 mmol) was added dropwise. The reaction flask was sealed with a septum and kept under an inert atmosphere using a balloon filled with argon. The mixture was stirred at room temperature overnight (18 h), and then refluxed at 80 °C for one hour. The product was purified by filtration with a $PTFE$ 0.44 μm membrane. The reaction mixture was filtered and washed with 100 mL acetone and 200 mL DMF, briefly sonicated (30 s), and filtered. This procedure was repeated three times (until the filtrate was clear). Finally, the product was washed with diethyl ether and dried in an oven at 60 °C for 12 h under a vacuum.

2.2.4. Synthesis of poly(methyl methacrylate) from graphene oxide surface (GO-g-PMMA)

Graphene oxide particles (200 mg) modified with initiator ($GO-BiBB$), $CuBr_2$ (1.56 mg, 0.0070 mmol) and $CuBr$ (6.0 mg, 0.042 mmol) were placed into a 100 mL Schlenk flask, evacuated, and backfilled with argon three times. The anisole (10.0 mL) and monomer (10 mL, 0.047 mmol) were purged with argon and then added to the reaction flask under argon flow. The initiator $EBiB$ (0.0121 mL, 0.047 mmol) in anisole (1 mL) was taken from a stock solution, purged with argon, and added to the reaction flask under argon flow. Similarly, $PMDETA$ (0.0098 mL, 0.047 mmol) in anisole (1 mL) was taken from a purged stock solution and added. The reaction was started by immersion of the flask in an oil bath preheated to 70 °C. The polymerization was stopped by opening the flask at 10% monomer conversion (as measured by 1H NMR) and the molecular weight was determined from the sacrificial initiator. The reaction mixture was diluted with acetone (30 mL) and filtered over 0.45 pm $PTFE$ filters. The $GO-g-PMMA$ was dispersed in DMF (100 mL), filtered, and washed with acetone (100 mL). This procedure was repeated three times. Finally, the $GO-g-PMMA$ was washed with diethyl ether (10 mL), dried at ambient temperature overnight, and then for 4 h at 60 °C in a vacuum oven (10 mbar). The general methodology of hybrid particles synthesis is presented in **Scheme 1**.

2.3. Methods

The GPC measurements were performed with a Wyatt (Wyatt, Dernbach, Germany) instrument equipped with two Perfect Separation Solutions (PSS) columns and one guard column ($GRAM$ Linear 10 (μm, M_n between 800 and 1000,000)), differential refractometer (RI) and light scattering (LS) detectors. The measurements were performed using DMF as eluent, containing 50 mmol $LiBr$, at a flow rate of 1 mL/min. $PMMA$ standards (M_n = 440-1650,000 g/mol) were used. Fourier transform infrared spectroscopy ($FTIR$) was used for the characterization of specific functional groups of the samples. The measurements were conducted in the mid-infrared region of 4000-650 cm^{-1} with 32 scans using $FTIR$ Nicolet 6700 spectrophotometer and $OMNIC$ 3.2 software (Thermo Scientific Products: Riviera Beach, FL, USA). The ATR accessory equipped with a single reflection diamond ATR crystal on ZnSe plate was used for all analyses. Thermogravimetry (TGA) was employed to study the polymer content in the polymer hybrid. Measurements were performed using a $TGA/DSC1$ analyzer (Mettler Toledo, Greifensee, Switzerland). Measurements were carried out in an argon atmosphere (flow rate 10 mL/min), in the temperature range of 25-600 °C, with a heating rate of 5 °C/min. All samples for rheological measurement were prepared in the form of films. For each sample, the total weight of the sample was 0.4 g, chloroform was used as a solvent (2 mL). Dissolved materials were cast on a petri dish (5 cm diameter) and left for 3 days at room temperature to let the solvent evaporate.

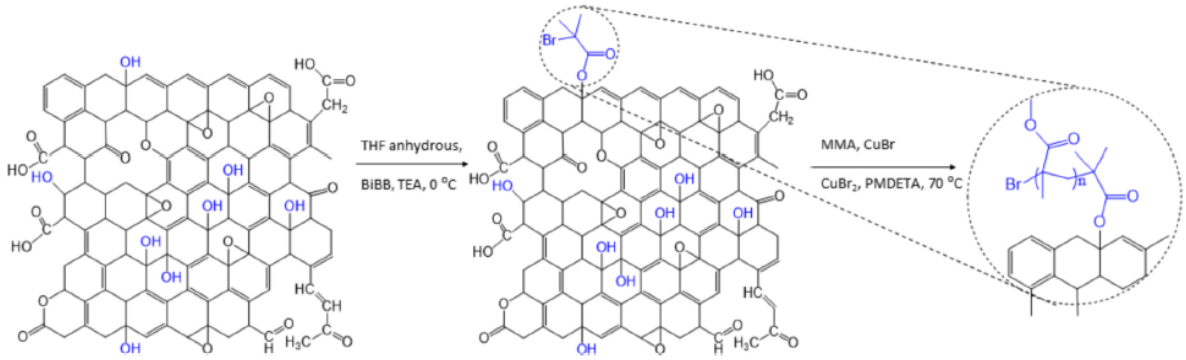

Scheme 1. Modification of graphene oxide with $ATRP$ initiator and grafting $PMMA$ from the GO surface.

After that, samples were dried in a vacuum oven at 40 °C, and 10 mbar for 2 days. Dynamic measurements of viscoelastic properties were carried out using an oscillation rotational rheometer Ares $G2$, TA Instruments (USA), two parallel plate geometry with a plate diameter of 25 mm was used. Temperature sweep measurements were conducted in constant angular frequency (ω) 0.1 rad s^{-1}, constant strain 1%, over a temperature range from 150 °C to 230 °C. Frequency sweep measurements were conducted under constant strain 1%, constant temperature 210 °C, in an angular frequency range from 0.1 to 621 rad s^{-1}. The morphology and droplet size of the polymer blends were analyzed using a transmission electron microscope (TEM; microscope: Tecnai Spirit $G2$ Twin; FEI, Brno, Czech Republic). The ultrathin sections for TEM observation were prepared by means of ultramicrotomy at room temperature (ultramicrotome EM UC7; Leica, Vienna, Austria). Before the TEM observation, the ultrathin sections were stained for 2 h in RuO_4 vapors to increase the contrast between the SAN phase (darker after RuO_4 staining) and $PMMA$ phase (brighter after RuO_4 staining) as described elsewhere [**2**]. The morphology of the polymer blend was visualized by bright field imaging (BF) at an accelerating voltage of 120 kV. Contact angle measurements were performed according to EN 828:2013 using goniometer OCA 15EC, Dataphysics (Germany) at room temperature. A defined volume (1.2 μL) of the following liquids: deionized water (DI), diiodomethane (DIM), ethylene glycol (EG), were deposited

from a dosing syringe onto the surface of the sample for the measurement. At least eight measurements were taken in different areas of each sample.

3. Results and discussion

Our previous work demonstrated that well-defined hybrid particles present in small quantities within polymer blends may induce significant changes in the blend's properties because of their performance as both compatibilizers and active fillers. [**26**] As a result, both the morphology of the blends, as well as the viscoelastic and mechanical properties were affected. It was demonstrated that the molecular weight of the tethered chains, the grafting density of the chains on the surface, the hybrid content, as well as the interaction between the blend' s components, played a crucial role in blend performance. Herein, blends of poly (styrene-co-acrylonitrile) and poly(methyl methacrylate) ($SAN/PMMA$) containing poly(methyl methacrylate) grafted on graphene oxide particles ($GO-g-PMMA$) were designed in such a way that the compatibili-zation effect of the hybrid particles within the $PMMA$ matrix was tuned via the molecular weight of both the matrix and grafted $PMMA$ chains. Two scenarios were expected; a) when $PMMA$ chains grafted onto the GO surface were longer than the matrix $PMMA$ they could be interpenetrated by the polymer matrix leading to better compatibility between the hybrid particles and the PMMA phase; b) when the chains on the surface were shorter than the matrix $PMMA$ the incompatibility was expected to be enhanced. Two blend compositions were investigated within the current studies: $SAN/PMMA$ = 70/30 and 90/10 wt/wt, while the hybrid content was held low at 1 wt%, similar to our previous systems.

3.1. Characterization of GO-g-PMMA hybrids

Surface-initiated atom transfer radical polymerization ($SI-ATRP$) was used for the synthesis of the hybrid particles containing poly(methyl methacrylate) grafted on the graphene oxide particles, $GO-g-PMMA$. Polymerization of methyl methacrylate was monitored by the evolution of the molecular weight of the free $PMMA$ generated from free initiator present within the reaction mixture. $PMMA$ with three different molecular weights was synthesized, M_n = 5600; 27,300, and 191,600 g/ mol. Molecular weights and their dispersity are given in **Table 1**. Narrow dispersity (Đ) values confirmed the polymerizations were well-controlled and resulted in well-defined materials. The structure of the hybrid particles was confirmed by $FTIR$ and TGA. **Fig. 1**a shows the $FTIR$ spectra of neat GO particles and synthesized hybrids which differ with the molecular weight of the tethered chains. The characteristic peaks at 3394 cm^{-1} ($O-H$ stretching), 1713 cm^{-1} ($C=O$ stretching), 1612 cm^{-1} ($C=C$ of aromatic ring stretching), 1360 cm^{-1} ($C-OH$ of carboxyl stretching), and 1054 cm^{-1} ($C-O$ epoxy stretching) could be assigned for the GO particles. After the modification of GO with $PMMA$ chains, a new absorption peak at 2948 cm^{-1} ($C-H$ stretching) could be observed. Furthermore, the intensity of peaks at ~1700 cm^{-1} was higher ($C=O$ stretching), and peaks at ~1385 cm^{-1} (-CH_3 stretching) attributed to $PMMA$ could be observed, which indicates that polymer was present on the particle surface. In addition, a characteristic peak at 1245 cm^{-1} can be observed ($C-C$ stretching) [**27,28**]. Based on TGA measurements (**Fig. 1**b) of neat GO and $GO-g-PMMA$, the content of the $PMMA$ grafted on the GO surface was determined to vary from 22 wt% in the case of small molecular weight $PMMA$ (M_n = 5600 g/mol) to 32 wt% for the hybrids with the highest $PMMA$ molecular weight (M_n = 191, 600 g/mol), [**28**]. The detailed values are collected in **Table 1**.

3.2. Morphology of the SAN/PMMA blends

The SAN polymer used within this study for the preparation of $SAN/PMMA = 70/30$ and $SAN/PMMA = 90/10$ blends contained 20.3 wt% of AN, and its molecular weight was $M_n = 209{,}200$ g/mol. According to literature data, such an AN content is in the range required for the formation of the single-phase material and miscible $SAN/PMMA$ blend [**29**]. The molecular weight of the matrix $PMMA$ was $M_n = 20$, 100 g/mol and $M_n = 130{,}900$ g/mol. The matrix-droplet morphology of the blends was observed. The presence of two immiscible phases was confirmed for all $SAN/PMMA$(20k)= 70/30 and $SAN/PMMA$(20k,130k) = 90/10 blend compositions. For immiscible polymer blends, nanoparticles can act as compatibilizers that are able to refine the phase size and stabilize the phase morphology. Usually, nanoparticles tend to be selectively located within one of the polymer phases, including dispersed and continuous phases.

Table 1 GPC characterization of poly(styrene-co-acrylonitrile) SAN, linear poly(methyl methacrylate) $PMMA$, and $PMMA$ synthesized in solution while grafting $PMMA$ on the GO surface, $GO-g-PMMA$.

Polymer	Abbreviation	Molecular weight (g/mol)	Dispersity $Đ$	Content of organic fraction
poly(styrene-*co*-acrylonitrile)	SAN	$M_n = 209{,}200$	1.30	-
poly(methyl methacrylate)	PMMA - 20k	$M_n = 20{,}100$	1.12	-
	PMMA – 130k	$M_n = 130{,}900$	1.07	-
GO-*g*-PMMA	PMMA- 6k	$M_n = 5600$	1.23	22%
	PMMA- 27k	$M_n = 27{,}300$	1.17	24%
	PMMA- 190k	$M_n = 191{,}600$	1.09	32%

The selective localization of nanofillers can be affected by various factors; two main factors being thermodynamic and kinetics effects. The thermodynamic effect relates to the particles tendency to minimize the interfacial energy through migration to the location with the strongest affinity and in this way to achieve an equilibrium state of dispersion. From the thermodynamic point of view, it is possible to predict the location of the filler by the analysis of calculated wetting coefficient according to the **Eq. 1**:

$$\omega = \frac{\gamma_{S-2} - \gamma_{S-1}}{\gamma_{12}} \qquad (1)$$

where, $ys-1$, $\gamma S-2$ and $\gamma 12$ represent the interfacial tension between the particles and polymer 1, the particles and polymer 2, and the two polymers 1 and 2, respectively. If $\omega > -1$, the particles are mainly located in polymer 1; if $\omega <$ — 1, the particles are distributed within polymer 2, and if — $1 < \omega < 1$, the particles are situated at the interface between polymer 1 and polymer 2 [**30**]. The kinetic effects are influenced by the processing procedures, while the shape and aspect ratio of the particles and can lead to a non-equilibrium distribution state of the nanoparticles. To examine the wetting coefficient and to predict the theoretical location of the nanoparticles the interfacial energy for polymer-polymer and polymer-nanoparticles interfaces were calculated based on two models: the geometric mean equation (**Eq. 2**) and the harmonic mean equation (**Eq. 3**) [**31**]:

$$\gamma_{12} = \gamma_1 + \gamma_2 - 2(\sqrt{\gamma_1^d \gamma_2^d} + \sqrt{\gamma_1^p \gamma_2^p} \quad (2)$$

$$\gamma_{12} = \gamma_1 + \gamma_2 - 4\left(\frac{\gamma_1^d \gamma_2^d}{\gamma_1^d + \gamma_2^d} + \frac{\gamma_1^p \gamma_2^p}{\gamma_1^p + \gamma_2^p}\right) \quad (3)$$

The dispersive γ^d and polar γ^p components of the solid surface tension y were calculated based on the contact angle measurements. The values of yd and yp components, and γ, $\gamma 12/21$ are given in **Table 2** and **Table 3**.

The tethering of the $PMMA$ chains onto the GO surface decreased the overall surface tension when compared to unmodified GO, **Table 2**. The calculated values of the interfacial tension between hybrid $GO - g - PMMA$ and $PMMA$ or SAN were significantly lower than between unmodified GO and SAN or $PMMA$, **Table 3**. The change in the affinity between the nanoparticles and polymer components after particle surface modification can lead to changes in the localization of the modified filler. Predicted theoretically, based on the values of the wetting coefficients, the selective localization of GO nanoparticles changed from $PMMA$ in the case of neat GO to SAN or interphase when modified GO was used, **Table 4**.

Based on the analysis of the wetting coefficients it was concluded that the $GO - g - PMMA$(190k) hybrids with grafted $PMMA$ chains on the GO surface with higher molecular weights than the matrix $PMMA$ (130k) were expected to be present at the interphase. But when the molecular weight of the hybrid and the matrix was decreased to $GO - g - PMMA$(27k) and matrix $PMMA$ (20k), respectively, but the tethered chains were still longer than matrix, the hybrids particles were predicted to be located in the SAN phase. A similar effect was observed for $PMMA$ grafted onto spherical silica nanoparticles [**32**]. In this work the authors claimed that the hybrid particles became more hydrophilic as the length of the PMMA brushes grafted on the silica surface increased and that their surface energy was very similar to the matrix $PMMA$. Due to the chain end effect, particles with short chains demonstrated increased dispersive component of surface energy that generated higher surface tension when incorporated into the $PMMA$ phase and increased affinity to the SAN phase. Here, the aspect ratio of the particles should also be considered because plate-like particles generate different interface contact when they are located at the interphase vertically or horizontally. Long brushes, due to the chain entanglements with free PMMA chains, should promote the vertical orientation along the interphase as is shown in the proposed model, **Scheme 2**.

Although the theoretical models can predict the particles' location, in most cases the dispersion of particles is in a non-equilibrium state, being affected by the processing conditions e.g., mixing, which can affect the migration of the nanoparticles from one phase to another. TEM studies confirmed the formation of an immiscible droplet morphology for all formulations, **Fig. 2**. Moreover, the presence of nanoparticles could lead to a change in the bulk viscosity of the blends and thus influence on the formation of the droplets.

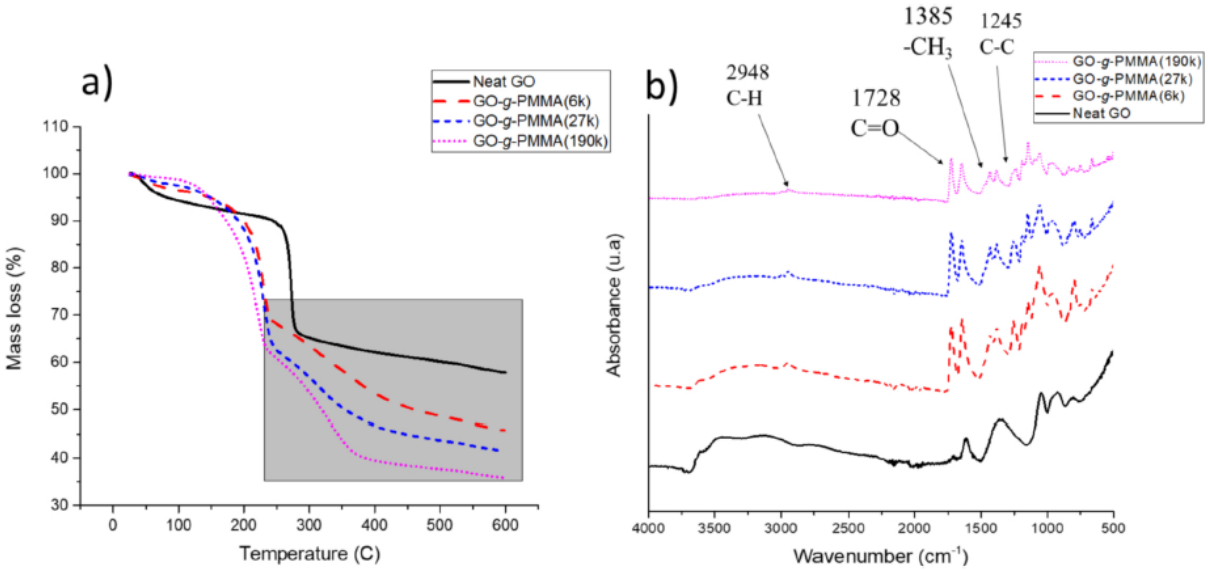

Fig. 1. TGA and $FTIR$ measurements for neat GO and $GO-g-PMMA$ hybrids.

Table 2 The dispersive and polar components of the overall solid surface tension (mN/m).

Sample	γ^d	γ^p	γ
SAN3	38.29	1.37	39.66
PMMA(20k)	28.46	7.49	35.95
PMMA(130k)	31.35	4.54	35.89
GO neat	32.44	33.9	66.35
GO-g-PMMA(6k)	55.63	2.14	57.77
GO-g-PMMA(27k)	53.45	3.09	56.53
GO-g-PMMA(190k)	31.19	1.05	32.23

Table 3 Interfacial tension between the particles and polymers or two polymers (mN/m).

Component 1	Component 2	γ_{12} (Eq. 2)	γ_{12} (Eq.3)
PMMA(20k)	SAN	3.18	5.67
PMMA(130k)	SAN	1.27	2.39
GO neat	SAN	21.89	30.50
GO-g-PMMA(6k)	SAN	1.70	3.37
GO-g-PMMA(27k)	SAN	1.60	3.16
GO-g-PMMA(190k)	SAN	0.37	0.76
GO neat	PMMA(20k)	9.66	17.12
GO-g-PMMA(6k)	PMMA(20k)	6.13	11.75
GO-g-PMMA(27k)	PMMA(20k)	4.85	9.44
GO neat	PMMA(130k)	13.65	22.45
GO-g-PMMA(190k)	PMMA(130k)	1.21	2.17

Table 4 The wetting coefficient values and predicted localization of the particles.

Particle	Matrix	ω (Ex.2)	ω (Ex.3)	Location
GO neat	PMMA(20k)/SAN	3.845	2.357	PMMA
GO-g-PMMA(6k)	PMMA(20k)/SAN	-1.394	-1.477	SAN
GO-g-PMMA(27k)	PMMA(20k)/SAN	-1.024	-1.108	SAN
GO neat	PMMA(130k)/SAN	6.498	3.363	PMMA
GO-g-PMMA(190k)	PMMA(130k)/SAN	-0.661	-0.590	interphase

The TEM studies showed that the droplet size depends not only on the blend composition, $SAN/PMMA$(20k)= 70/30 vs $SAN/PMMA$ (20k)= 90/10 (**Fig. 2**. Samples A1, B1) but also on the molecular weight of the matrix $PMMA$, $SAN/PMMA$(130k)= 90/10 (**Fig. 2**. Sample C1). A smaller diameter of $PMMA$ droplets was observed for the matrix PMMA with a higher molecular weight (130k) (**Fig. S1.**). This correlates with the values of surface tension (**Table 3**), as lower values were calculated for the composition $SAN/PMMA$ (130k). A more homogenous distribution of droplet size and a smaller droplet diameter for $SAN/PMMA$ (130k)= 90/10 blends result from a similar molecular weight of both components, SAN and $PMMA$, generating lower surface tension during mixing that influences the coarsening of the droplets during blend preparation.

The images of the blends containing the hybrid particles $SAN/PMMA$ (20k)/$GO-g-PMMA$(6k)/(20k) = 70/30, justified the above scenario by the correlation of the molecular weight of the grafted $PMMA$ with the molecular weight of the matrix $PMMA$ impacting the formation of droplets. Larger diameter $PMMA$ domains were formed if the tethered PMMA chains on the GO surface were not penetrated by the $PMMA$ matrix, $GO-g-PMMA$(6k). Opposite, when the surface-grafted $PMMA$ chains were interpenetrated by the chains of the $PMMA$ matrix the compatibilization of $SAN/PMMA$(20k)/$GO-g-PMMA$(27k) was observed and smaller domains of the $PMMA$ dispersed phase were formed. Moreover, the length of the grafted chains affected the location of the $GO-g-PMMA$ filler, as confirmed by the analysis of the wetting coefficient. The hybrid fillers with the shortest grafted $PMMA$ chains were mostly localized outside the $PMMA$ droplets thus the interaction with $PMMA$ phase were constrained. The presence of the modified particles at the interphase was crucial in resticting the coalescence of the droplets. This effect was well-visible for systems with $SAN/PMMA$(130k) = 90/ 10. A much smaller diameter of $PMMA$ droplets in comparison to other systems were formed, although not very homogenous. Still, this confirmed the location at the interphase and that the wettability of the tethered $PMMA$ by free $PMMA$ chains was crucial for the reduction in droplet diameter. The influence of both neat GO and the $GO-g-PMMA$ hybrids on blend morphology was further analyzed by rheological studies.

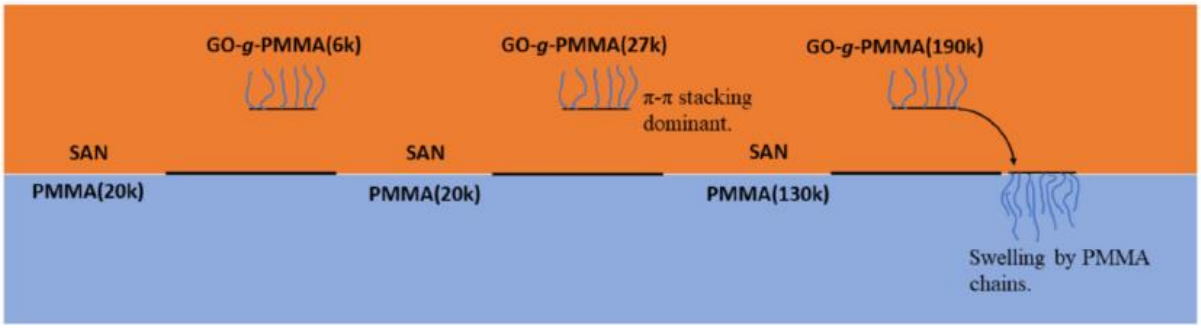

Scheme 2. Compatibilization effect by the addition of polymer grafted graphene oxide particles.

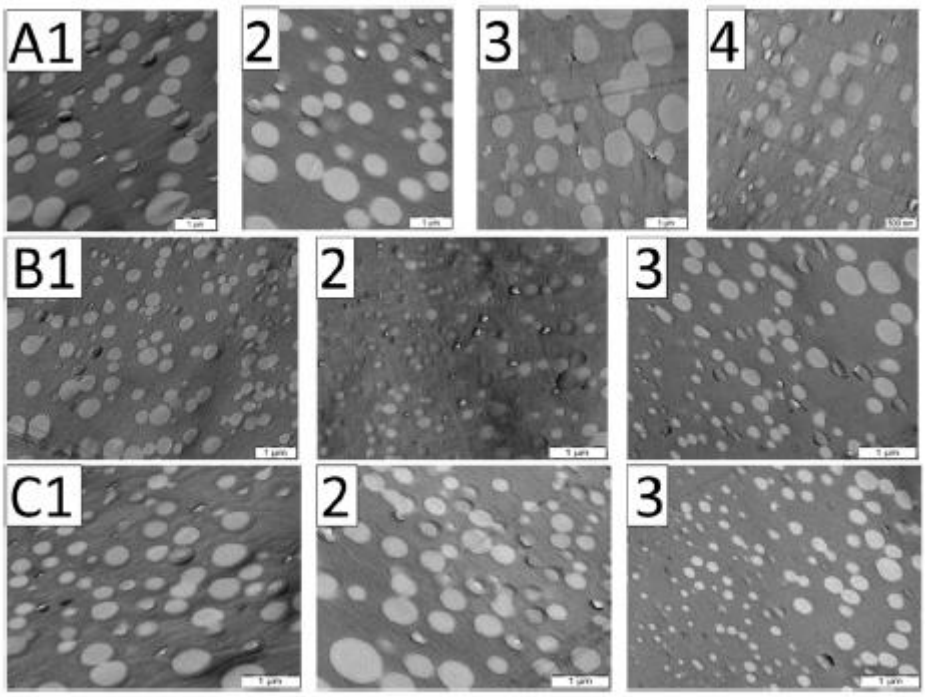

Fig. 2. TEM micrographs for different $SAN/PMMA$ blends, A) (1) $SAN/PMMA$ (20k) = 70/30, (2) $SAN/PMMA$(20k)/GO, (3) $SAN/PMMA$(20k)/$GO-g-PMMA$ (6k), (4) $SAN/PMMA$(20k)/$GO-g-PMMA$(27k) B) (1) $SAN/PMMA$(20k) = 90/ 10, (2) $SAN/PMMA$(20k)/GO, (3) $SAN/PMMA$(20k)/$GO-g-PMMA$(27k), C) (1) $SAN/PMMA$(130k) = 90/10, (2) $SAN/PMMA$(130k)/GO, (3) $SAN/PMMA$ (130k)/$GO-g-PMMA$(190k).

3.3. Rheological performance

3.3.1. Basic viscoelastic properties of SAN/PMMA blends

Dynamic temperature sweep tests were performed within the linear viscoelastic regime at a low frequency 0.1 rad s^{-1} in the temperature range of 150-230 °C. In the case of pure $SAN/PMMA$(20k) = 70/30 blends the values of the loss modulus G'' were higher than storage modulus G' in the whole studied temperature range which indicated viscous behavior of the blends (Fig.S2).

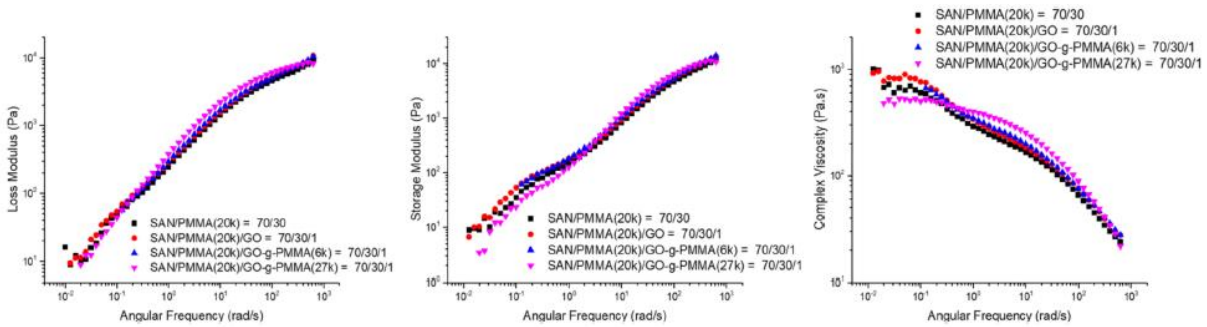

Fig. 3. The viscoelastic properties of $SAN/PMMA$ blend, $SAN/PMMA$ = 70/30. The values of the storage shear modulus G', loss shear modulus G'' and complex viscosity η^* measured during frequency sweep tests at 210 °C, applied oscillation amplitude 1%.

The presence of neat GO did not affect these properties; a similar decrease in G' and G'' values was found as the temperature increased. However, the values of G' and G'' were significantly different for both blends containing hybrid particles, $GO-g-PMMA$(6k) and $GO-g-PMMA$(27k), and higher

in a case of hybrids wetted by matrix $PMMA$. A similar trend was observed in the case of complex viscosity η^* versus temperature plots (**Fig. S3**). Therefore, it was concluded that the presence of $GO-g-PMMA$ with tailored molecular weights affected the melting behavior of the blends.

Based on the temperature sweep tests a temperature of 210 °C was chosen to study the viscoelastic behavior of the blends as a function of angular frequency, especially since the temperature 230 ° C is considered to be the ceiling temperature for $PMMA$ [2]. The frequency sweep tests at 210 °C and the values of storage shear modulus G, loss shear modulus G' and complex viscosity η^* are shown in **Fig. 3**. The cross points of the storage modulus G' and loss modulus G'' determined based on the frequency sweep test are compiled in **Table 5**.

It can be seen that the dependence between the storage and loss moduli and angular frequency for the blends of $SAN/PMMA$ = 70/30 containing GO or $GO-g-PMMA$ particles were quite similar, **Fig. 3**. The contribution of the hybrid particles within the blend on its properties was enhanced when the content of the $PMMA$ matrix was decreased when compared to SAN content, $SAN/PMMA$ (20k, 130k) = 90/10, again 1 wt% of hybrid particles were added. This means the content of the $PMMA$ tethered on the surface of the particles within the matrix $PMMA$ was much higher when compared to $SAN/PMMA/GO-g-PMMA$ = 70/30/1. In this case the molecular weight of the matrix $PMMA$ was Mn = 20,100 and Mn = 130,900 g/mol. But the molecular weight of $PMMA$ grafted on the GO surface was higher than that used as matrix $PMMA$ (M_n = 27,300 and 191,600 g/mol), providing miscibility of the matrix $PMMA$ and grafted $PMMA$ chains. In this case the incorporation of GO into the $SAN/PMMA$ (20k, 130k) = 90/10 blend enhanced the values of the storage modulus at high frequencies thereby indicating a reinforcing effect of the solid particles (**Fig. 4**.).

Table 5 The values of angular frequency (rad/s), the storage shear modulus G' and loss shear modulus G'' (Pa) at cross points (G'=G'') and mean relaxation times τ (s) calculated based on Cole-Cole plots.

Sample composition	Matrix ratio	Crossover point (kPa)	Crossover point (rad/s)	τ (s)
SAN/PMMA(20k)	70/30	4.62	98.66	0.081
SAN/PMMA(20k)/GO		4.94	86.97	0.083
SAN/PMMA(20k)/GO-*g*-PMMA(6k)		4.61	74.56	0.087
SAN/PMMA(20k)/GO-*g*-PMM(27k)		5.58	77.17	0.094
SAN/PMMA(20k)	90/10	3.35	86.97	0.085
SAN/PMMA(20k)/GO		7.77	79.57	0.099
SAN/PMMA(20k)/GO-*g*-PMMA(27k)		4.78	85.48	0.109
SAN/PMMA(130k)		8.53	43.46	0.112
SAN/PMMA(130k)/ GO		9.87	41.77	0.125
SAN/PMMA(130k)/ GO-*g*-PMMA(190k)		2.25	44.80	0.077

The effect was more significant for the $SAN/PMMA$ = 90/10 blend when lower molecular weight matrix $PMMA$ (20k) was used. A reduction of the storage shear modulus G and loss modulus G were observed when the hybrid particles were added when compared with neat GO particles. The incorporation of GO particles and GO hybrids shifted the values of the frequency at which the cross

points $G' = G$ were observed. (**Table 5**). The predominant viscous behavior for neat blends, independently of the $SAN/PMMA$ ratio, started at higher values of frequency. The addition of GO enhanced the elastic behavior, and the cross-points were determined at lower frequency values when compared with neat $SAN/PMMA$ materials of a similar composition.

The plateau of the complex viscosity η^* at low frequencies was well-defined only for the $SAN/PMMA$(20k) = 70/30 blend containing $GO-g-PMMA$(27k), and it started at a higher frequency value than for other $SAN/PMMA$(20k) = 70/30 based blends (**Fig. 3**.). Moreover, the blend with the higher molecular weight of $PMMA$(27k) showed more distinct shear thinning behavior at the power law region; the stronger reduction of the complex viscosity values was observed as the frequency and shear rate increased. If the SAN content within the blend was higher ($SAN/PMMA$ = 90/10) the effect of the matrix $PMMA$ molecular weight on the complex viscosity values η^* at the plateau was not strongly pronounced. The incorporation of GO particles caused an increase in the values of the complex viscosity η^* at a higher frequency range no matter the molecular weight of the matrix $PMMA$, when compared with neat $SAN/PMMA$ = 90/10 (**Fig. 4**.). This was observed because the solid additives could generate a hydrodynamic effect and increase the viscosity. Furthermore, they also could affect the melting rate of the polymer due to their different thermal conductivity. On the contrary, when the hybrid particles were added, a significant reduction in complex viscosity was observed i.e., the grafted chains plasticized the matrix. This effect was much stronger if the high molecular weight of both matrix ($PMMA$ (130k)) and grafted ($PMMA$(190k)) chains was investigated.

3.3.2. The influence of the particles on the compatibility of the blend

Chopra D. et al. [**3**] showed that the phase separation temperature of poly(styrene-co-maleic anhydride)/poly(methyl methacrylate blends) was marked by a change in the slope of the elastic modulus and the presence of the maximum in tan δ values measured as a function of temperature. The quantitative detection of phase separation temperatures based on the elastic modulus for all compositions ($SAN/PMMA$ (20k/130k) = 70/30 and 90/10) was not possible, as the observed changes in the slope of G' were subtle. However, the tan δ peaks were used for qualitative comparisons of the rheological behavior of various compositions of $SAN/PMMA$ blends.

The formation of the well-defined tan δ peaks occurred for $SAN/PMMA$(20k) = 70/30 and for $SAN/PMMA$(20k) = 90/10. As shown in **Fig. S4**, the behavior of the pure blend $SAN/PMMA$(20k) = 70/30 demonstrates the higher values of tan δ as compared with blends containing GO-g-PMMA(6k) and neat GO. No clear peaks of tan 8 were observed for this system after incorporation of GO or $GO-g-PMMA$(6k). Conversely, in the case of higher molecular weights of the grafted $PMMA$, $GO-g-PMMA$(27k), the highest values of tan 8 were detected for blends containing hybrid particles. Similar effects were observed for $SAN/PMMA$(20k)/$GO-g-PMMA$(27k) = 90/10/1. In this case the incorporation of the hybrid $GO-g-PMMA$ (27k) into $SAN/PMMA$ (20k) = 90/10 increased the values of tan δ. No well-defined peaks on tan δ plots were observed for the $SAN/PMMA$(130k) = 90/10 blends. The tan δ values continuously increased alongside the temperature values. The observed differences in maximum of tan delta are not due to phase separation but rather due to a change of the relaxation time of the droplets. The fluctuation of the points was primarily due to inhomogeneous distribution and differences in the size of the $PMMA$ droplets, which was confirmed by the TEM analysis.

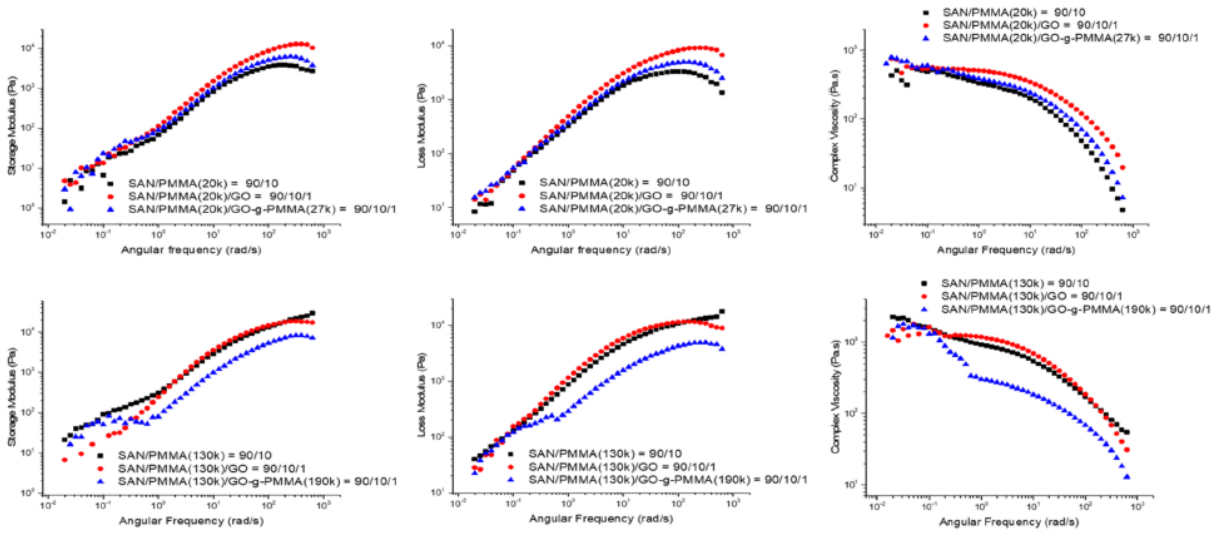

Fig. 4. The viscoelastic properties of $SAN/PMMA$ blend, $SAN/PMMA$ = 90/10. The values of the storage shear modulus G', loss shear modulus G'' and complex viscosity n^* measured during frequency sweep tests at 210 ° C, applied oscillation amplitude 1%.

Better quantification of the differences that correspond with the rheological behavior of the miscible and immiscible blends can be obtained using van Gurp-Palmen plots, viscosity Cole-Cole plots, and relaxation spectra [**33,34**]. The van Gurp and Palmen plot (vGP plot) is a plot of the phase angle δ (◦) versus the magnitude of the complex modulus [G^*] [**33-35**].

The presence of the maximum on the vGP plots and the valley for the low values of [G^*] for all investigated systems indicates immiscibility and droplet-matrix morphology regardless of the composition of the blend (**Fig. 5**). However, the changes formed in the shape of the vGP plots were strongly influenced by the composition of the blend matrix, the presence of particles, as well as the molecular weight of the tethered $PMMA$ on GO. On the vGP plots of $SAN/PMMA$(20k) = 70/30 blends a strong visible maximum and a valley for the lower values of [G^*] were formed. Further, no meaningful influence on the shape of the vGP plots occurred after the incorporation of GO or hybrid $GO-g-PMMA$(6k). But if the molecular weight of the matrix and grafted PMMA on the GO surface were compatible, the maximum of vGP plot was significantly shifted to lower values of [G^*] when compared to blend containing neat GO. The vGP plots of $SAN/PMMA$(20k) = 90/10 showed a more similar shape to that observed for the homogenous linear polymers, and a plateau was observed due to various ratio of $SAN/PMMA$. Both GO and hybrid particles increased the values of [G^*] measured for low values of phase angle δ (◦) due to a reinforcing effect. Molecular weight of matrix $PMMA$ (130k) influenced on the viscoelastic behaviour of the $SAN/PMMA$ = 90/10 blend. The plateau formed after the addition of neat GO particles disappeared and a maximum on the vGP plot and a valley for the low values of [G^*] were formed. Here, the compatibilizing effect of neat GO was indicated, being reflected on the vGP plot via the plateau formed.

Fig. 6 shows the viscosity Cole-Cole plots for all investigated blends which demonstrate the presence of two phases differing in relaxation. The miscible, homogenous system shows only one circular arc on the viscosity Cole-Cole plots, while two arcs indicate a second relaxation mechanism and denote the formation of the second phase, respectively. The relaxation times were calculated based on the Cole-Cole plots and the formed first arc according to the method described in literature [**33**]. The calculated values are compiled in **Table 5**.

The Cole-Cole plots reflect the strong impact of the blend composition and molecular weight of $PMMA$. Phase separation of $SAN/PMMA$ (20k)/GO = 70/30/1 and $SAN/PMMA$(20k)/$GO-g-PMMA$(6k/27k) = 70/30/1 blends was confirmed by the shape of the Cole-Cole plots. Additionally, the two-phase morphology of these blends was observed by TEM studies. In the case of $SAN/PMMA$ = 70/30, more visible semicircular arcs were observed for systems with a higher molecular weight of tethered $PMMA$ (M_n = 27,300 g/mol).

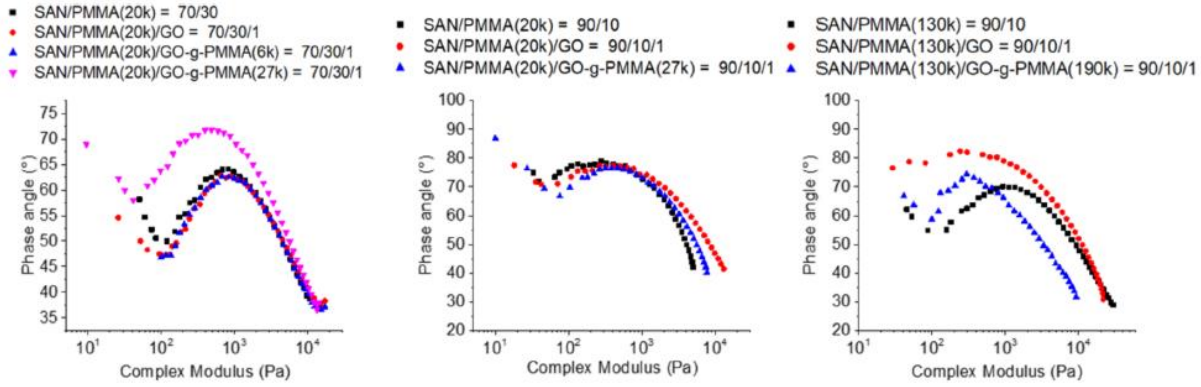

Fig. 5. The vGP plots for $SAN/PMMA$ blends.

The beginning of the formation of the second peak was visible in this case for higher values of η', indicating the presence of two phases. The higher compatibility and homogeneity of that blend occurred due to the appropriate range of $PMMA$ molecular weights for the matrix and tethered $PMMA$. However, the lower molecular weight of $PMMA$ in comparison to SAN; M_n = 20,100 g/mol caused stronger differences in viscosity between those components reflected by the characteristics of the Cole-Cole plot, which led to the formation of various size droplets. Both, GO and $GO-g-PMMA$ (6k/27k) shifted the maximum of the second relaxation peak compared with the neat $SAN/PMMA$ (20k) = 70/30 blend indicating the influence of the additives on the formation and size of the $PMMA$ droplets, as was confirmed by TEM analysis. The calculated mean relaxation times (**Table 5**) for $SAN/PMMA$(20k) = 70/30 showed that the incorporation of GO and $GO-g-PMMA$ slightly increased the values of τ.

The calculated values of the mean relaxation times t increased after the incorporation of GO and the $GO-g-PMMA$ hybrid into $SAN/PMMA$ (20k/130k) = 90/10. Tails forming second circular arcs were observed for such blends indicating the different internal structures of the dispersed phase. In the case of a low molecular weight PMMA matrix (20k), the presence of the hybrid particles enhanced the homogeneity only slightly, which was reflected by a very small shift of the first peak on the Cole-Cole plot indicating a longer relaxation time, as confirmed by the calculated values of the mean relaxation time τ (**Table 5**). This can be explained by the stronger interphase interaction generated between the $GO-g-PMMA$ and $PMMA$ droplets due to the possibility of the wetting of the surface of the hybrid particles by the matrix $PMMA$ chains and entanglement formation. A strong influence on the $SAN/PMMA$(20k) = 90/10 blend behavior was generated by the neat GO. Here, the semicircular peak is more visible indicating better homogeneity of the system. A similar effect of neat GO incorporation was observed for the $SAN/PMMA$(130k) = 90/10 blend. The maximum of the peaks occurred at lower frequency values indicating longer relaxation times after the incorporation of the GO particles. Here, a significant increase in the calculated mean relaxation time τ when compared with neat $SAN/PMMA$(130k) = 90/10 was observed (**Table 5**). This can be explained by stronger interphase

interactions generated between the GO surface and the SAN matrix that can disturb the relaxation [**36**].

On the contrary, the Cole-Cole plot of the $SAN/PMMA$(130k)/$GO-g-PMMA$(190k) blend demonstrated a very narrow semicircular arc, followed by secondary arc formation. The first peak was formed at lower values of η' and displayed its maximum at higher frequency values indicating shorter relaxation times when compared to the neat $SAN/\ PMMA$(130k) = 90/10 blend. The calculated value of mean relaxation time t for $SAN/PMMA$(130k)/$GO-g-PMMA$ = 90/10/1 was significantly shorter. This reflects significant changes in the relaxation behavior of the $SAN/PMMA$(130k) = 90/10 blend after incorporation of the GO hybrid corresponding to the various relaxations of the matrix and droplets.

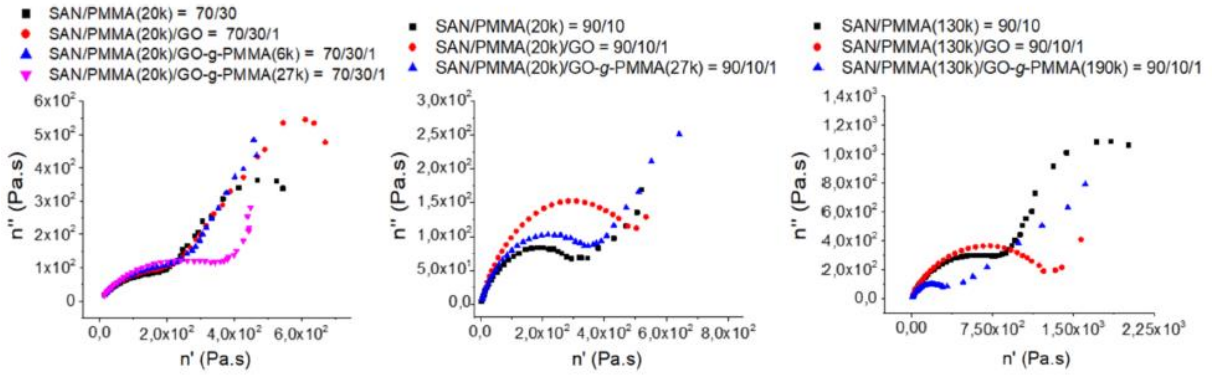

Fig. 6. Cole-Cole plots for $SAN/PMMA$ blends.

This could be the effect of two factors; a) the relaxation of the $PMMA$ droplets is facilitated due to the presence of the $GO-g-PMMA$ (190k) particles and the possibility of wetting the filler surface by the shorter matrix $PMMA$ chains; b) the long (190,000 g/mol) $PMMA$ chains tethered on the GO surface can fully screen the particle core reducing the possibility of $\pi-\pi$ interactions with the SAN phase which results in morphology changes due to different localizations of hybrid $GO-g-PMMA$ filler. According to the literature the "optimal" grafting density is needed to enhance homogenous dispersion of the hybrid particles throughout the matrix [**37**]. The long brushes can form entanglements with polymer matrix chains, but if their grafting density is low, they can form coils on the surface. Such mushroom-like formed morphologies reduce the efficiency of interactions with the matrix. Lack of n-n interactions of the hybrid particles present within the SAN phase can increase incompatibility but also can facilitate the relaxation of the SAN phase. Here, the previously described plasticizing effect of the $GO-g-PMMA$ particles present at the interphase and in the SAN phase is also important and can influence the relaxation of the matrix [**2**].

It was expected that the effect of the hybrid particles present in the blends could be enhanced by a higher particle content within the blend. Therefore, similar blends were prepared, but the particle content was increased to 5 wt%, $SAN/PMMA$(20k)/$GO-g-PMMA$(6k/27k) = 70/30/5. The molecular weight of the tethered chains was lower or higher when compared to the molecular weight of the $PMMA$ used as the matrix, leading to varied hybrids and linear $PMMA$ compatibility. As seen in **Fig. 7**, in the case of better compatibility between the matrix and grafted chains, when the tethered chains are longer (27k) and the content of particles is higher (5 wt%), the first semicircular arc is more visible and its maximum occurs at lower values η' (high values of frequency) indicating even more facilitated relaxation of the matrix due to stronger interphase separation caused by the presence of the $GO-g$-particles. On the other hand, the longer brushes tethered to the GO surface allowed the

shorter matrix $PMMA$ (20k) chains to penetrate the free space between the grafted chains to wet the surface of the GO particles. This stabilized the size and homogeneity of the $PMMA$ droplets. Further, due to stronger interphase interactions between the particles and $PMMA$ phase, and more homogenous dispersion, the relaxation of the droplets was also facilitated.

On the contrary, if the hybrids and linear $PMMA$ (20k) were less compatible, for example if the tethered chains were shorter (6k), the effect was opposite, and the first arc occurs at higher values η' for a higher content of hybrid particles thereby indicating longer relaxation times. The formation of the second arc is also strongly visible which confirms the immiscibility of the system. The maximum of the second peak is shifted to higher values of n and lower frequency values indicating a longer relaxation time. Densely grafted, short brushes can lead to worse dispersion due to the strong attractive force between particles and the reduced possibility of entanglement formation with the matrix chains [**38**] resulting in the formation of bigger $PMMA$ droplets with longer relaxation times.

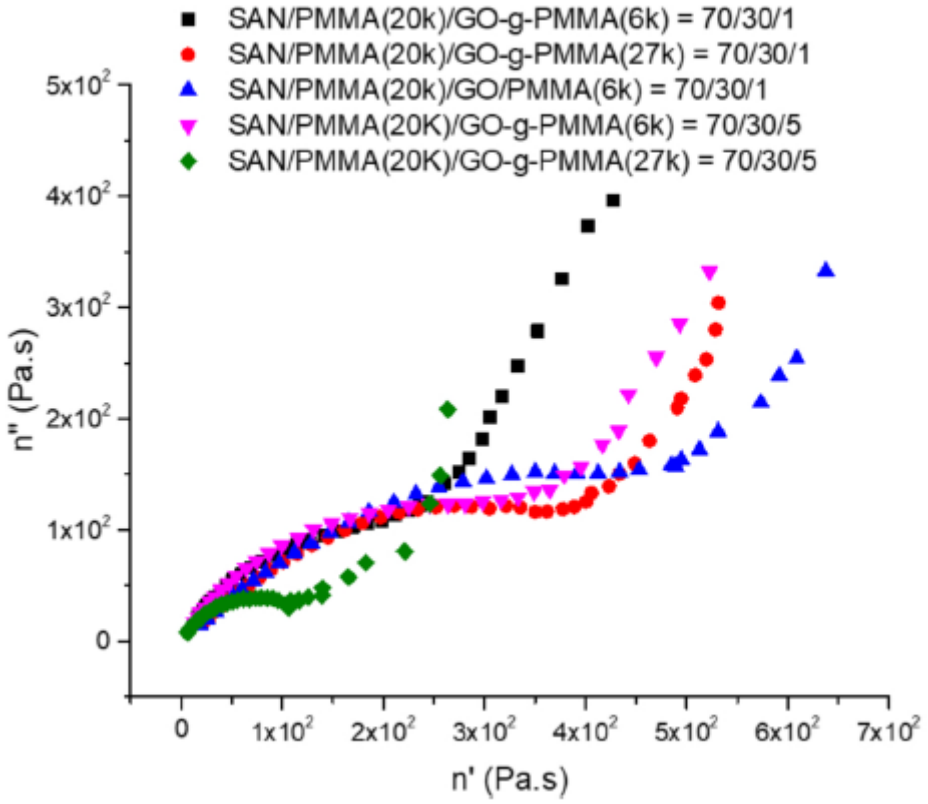

Fig. 7. Cole-Cole plots for $SAN/PMMA$ blends containing an increased amount of the hybrid particles.

Overall, it should be emphasized that the tethering of $PMMA$ chains on the GO surface had a tremendous effect on the blend behavior independent of the molecular weight of the $PMMA$ matrix and $PMMA$ tethered on the GO surface. That was confirmed by referring to a blend in which GO was added to the $SAN/PMMA$ blend with an additional amount of matrix $PMMA$ with a molecular weight corresponding to the grafted chains.

4. Conclusions

Well-defined hybrid particles of $GO - g - PMMA$ with molecular weights correlating to the molecular weight of the matrix $PMMA$ within $SAN/\ PMMA$ blends were demonstrated to affect the rheological performance and morphologies of the blends. Two ratios of SAN/PMMA blends; 70/ 30 and 90/10 and two molecular weights of matrix $PMMA$ (M_n = 20,100 or 130,900 g/mol) were chosen as representative compositions. The content of $GO - g - PMMA$ was 1 wt%.

Two different effects were confirmed via the rheological performance of the investigated blends. First, better compatibility of the components of the blends resulting from the wettability of the grafted long $PMMA$ chains by the shorter matrix $PMMA$ chains; and second, enhanced immiscibility generated by expelled longer matrix $PMMA$ from the hybrid particles containing grafted $PMMA$ chains that were shorter than the matrix. The analysis of Cole-Cole plots demonstrated the presence of two phases that differed in relaxation in all $SAN/PMMA$ compositions.

It was found that low molecular weight (20k) of the matrix $PMMA$ used to prepare the $SAN/PMMA$(20k)= 70/30 blend was a crucial factor influencing the composition's compatibility. The strong differences in viscosity of both blend components led to stronger phase separation and the formation of various diameters of PMMA droplets. This was reflected in the Cole-Cole plot shape. Here, the incorporation of both GO and $GO - g - PMMA$ did not cause significant changes in the character of the Cole-Cole plots and the calculated values of mean relaxation times τ (s).

The incorporation of GO changed the morphology of the $SAN/PMMA$ (20k, 130k)= 90/10 blends, as confirmed by TEM studies. The diameter of the PMMA droplets decreased. This effect was particularly visible for the blends based on lower molecular weight (20k) matrix $PMMA$. The presence of GO changed the viscoelastic behavior of the $SAN/PMMA$ (20k, 130k)= 90/10 blends due to the formation of n-n interactions with the SAN within the matrix. The calculated mean relaxation times t were longer when compared to the neat $SAN/PMMA$(20k, 130k) = 90/10 blend.

The presence of $GO - g - PMMA$(190k) significantly influenced the shape of the Cole-Cole plots determined for the $SAN/PMMA$(130k)= 90/10 blend. This facilitated relaxation and a shorter mean relaxation time t was observed due to the possibility of wetting the filler surface by the shorter matrix $PMMA$ chains.

References

[1] T. Ribeiro, C. Baleizao, J.P.S. Farinha, Functional films from silica/polymer nanoparticles, Materials 7 (2014) 3881-3900, **https://doi.org/10.3390/ ma7053881**.

[2] M. Ilcikova, M. Galeziewska, M. Mrlik, J. Osicka, M. Masar, M. Slouf, M. Maslowski, M. Kracalik, R. Pietrasik, J. Mosnacek, J. Pietrasik, The effect of short polystyrene brushes grafted from graphene oxide on the behavior of miscible PMMA/SAN blends, Polymers 211 (2020), 123088, **https://doi.org/10.1016/j. polymer.2020.123088**.

[3] D. Chopra, M. Kontopoulou, D. Vlassopoulos, S.G. Hatzikiriakos, Effect of maleic anhydride content on the rheology and phase behavior of poly(styrene-co-maleic anhydride)/poly(methyl methacrylate) blends, Rheol. Acta 41 (2002) 10-24, **https://doi.org/10.1007/s003970200001**.

[4] A.R. Ajitha, S. Thomas, Introduction: polymer blends, thermodynamics, miscibility. Phase ;Separation, and Compatibilization, Elsevier Inc., 2019, **https://doi.org/10.1016/B978-0-12-816006-0.00001-3**.

[5] D. Arthisree, G.M. Joshi, Graphene oxide derived high dielectric constant of polymer blends, Mater. Res. Express 5 (2018), **https://doi.org/10.1088/2053-1591/aad108**.

[6] Z. Fu, H. Wang, X. Zhao, S. Horiuchi, Y. Li, Immiscible polymer blends compatibilized with reactive hybrid nanoparticles: morphologies and properties, Polym. (Guildf.) 132 (2017) 353-361, **https://doi.org/10.1016/j. polymer.2017.11.004**.

[7] J.S. Reinaldo, L.M. Pereira, E. dos S. Silva, M.M. Ueki, E.N. Ito, Effect of the chemical structure on the linear viscoelastic behavior of acrylic and styrenic polymer blends, Polym. Test. 67 (2018) 257-265, **https://doi.org/10.1016/). polymertesting.2018.03.013**.

[8] G.N. Kumaraswamy, C. Ranganathaiah, M.V.D. Urs, H.B. Ravikumar, Miscibility and phase separation in SAN/PMMA blends investigated by positron lifetime measurements, Eur. Polym. J. 42 (2006) 2655-2666, **https://doi.org/10.1016/). eurpolymj.2006.05.007**.

[9] J. Resch, J. Dreier, C. Bonten, M. Kreutzbruck, Miscibility and phase separation in pmma/san blends investigated by nanoscale afm-ir, Polymers 13 (2021), **https:// doi.org/10.3390/polym13213809**.

[10] J. Parameswaranpillai, G. Joseph, S.K. Sidhardhan, S. Jose, N. Hameed, Miscibility, UV resistance, thermal degradation, and mechanical properties of PMMA/SAN blends and their composites with MWCNTs, J. Appl. Polym. Sci. 133 (2016) 1-11, **https://doi.org/10.1002/app.43628**.

[11] P. Xavier, P. Rao, S. Bose, Nanoparticle induced miscibility in LCST polymer blends: Critically assessing the enthalpic and entropic effects, Phys. Chem. Chem. Phys. 18 (2016) 47-64, **https://doi.org/10.1039/c5cp05852j**.

[12] T.V.M. Ndoro, E. Voyiatzis, A. Ghanbari, D.N. Theodorou, M.C. Bohm, F. Muller-Plathe, Interface of grafted and ungrafted silica nanoparticles with a polystyrene matrix: atomistic molecular dynamics simulations, Macromolecules 44 (2011) 2316-2327, **https://doi.org/10.1021/ma102833u**.

[13] V.V. Ginzburg, Influence of nanoparticles on miscibility of polymer blends. a simple theory, Macromolecules 38 (2005) 2362-2367, **https://doi.org/10.1021/ ma0482821**.

[14] G. Chen, P. Li, Y. Huang, M. Kong, Y. Lv, Q. Yang, G. Li, Hybrid nanoparticles with different surface chemistries show higher efficiency in compatibilizing immiscible polymer blends, Compos. Sci. Technol. 105 (2014) 37-43, **https://doi.org/ 10.1016/j.compscitech.2014.09.013**.

[15] N. Song, J. Yang, P. Ding, S. Tang, Y. Liu, L. Shi, Effect of covalent-functionalized graphene oxide with polymer and reactive compatibilization on thermal properties of maleic anhydride grafted polypropylene, Ind. Eng. Chem. Res. 53 (2014) 19951-19960, **https://doi.org/10.1021/ie5031985**.

[16] D.R. Paul, Interfacial agents ("Compatibilizers") for polymer blends, Academic Press, INC (1978), **https://doi.org/10.1016/b978-0-12-546802-2.50008-7**.

[17] G. Eda, M. Chhowalla, Chemically derived graphene oxide: towards large-area thin-film electronics and optoelectronics, Adv. Mater. 22 (2010) 2392-2415, **https://doi.org/10.1002/adma.200903689**.

[18] M. Nikdel, M. Salami-Kalajahi, M. Salami Hosseini, Synthesis of poly(2-hydroxyethyl methacrylate-co-acrylic acid)-grafted graphene oxide nanosheets via reversible addition-fragmentation chain transfer polymerization, RSC Adv. 4 (2014) 16743-16750, **https://doi.org/10.1039/c4ra01701c**.

[19] A. Kumar, A. Bansal, B. Behera, S.L. Jain, S.S. Ray, Ternary hybrid polymeric nanocomposites through grafting of polystyrene on graphene oxide-TiO2 by surface initiated atom transfer radical polymerization (SI-ATRP), Mater. Chem. Phys. 172 (2016) 189-196, **https://doi.org/10.1016/j.matchemphys.2016.01.064**.

[20] N. Rajender, K.I. Suresh, Surface-initiated atom transfer radical polymerization (SI-ATRP) from graphene oxide: effect of functionalized graphene sheet (FGS) on the synthesis and material properties of PMMA nanocomposites, Macromol. Mater. Eng. 301 (2016) 81-92, **https://doi.org/10.1002/mame.201500256**.

[21] F. Fenouillot, P. Cassagnau, J.C. Majeste, Uneven distribution of nanoparticles in immiscible fluids: morphology development in polymer blends, Polymers 50 (2009) 1333-1350, **https://doi.org/10.1016/j.polymer.2008.12.029**.

[22] W.H. Ferreira, C.A. Silva, C.T. Andrade, Improved compatibilization and shape memory properties of poly(3-hydroxybutyrate-co-3-hydroxyvalerate)/poly (ethylene-co-vinyl acetate) blends by incorporation of modified reduced graphene oxide, Polymers 201 (2020), 122625, **https://doi.org/10.1016/j. polymer.2020.122625**.

[23] P. Xavier, P. Rao, S. Bose, Nanoparticle induced miscibility in LCST polymer blends: Critically assessing the enthalpic and entropic effects, Phys. Chem. Chem. Phys. 18 (2016) 47-64, **https://doi.org/10.1039/c5cp05852j**.

[24] C. Botas, P. .Alvarez, P. Blanco, M. Granda, C. Blanco, R. Santamaría, L. J. Romasanta, R. Verdejo, M.A. López-Manchado, R. Menendez, Graphene materials with different structures prepared from the same graphite by the Hummers and Brodie methods, Carbon N. Y 65 (2013) 156-164, **https://doi.org/ 10.1016/j.carbon.2013.08.009**.

[25] M. Ilcikova, RSC Advances reduction of graphene oxide vs. catalysis of atom, (2015) 3370-3376. **https://doi.org/10.1039/c4ra12915f**.

[26] M. Zygo, M. Mrlik, M. Ilcikova, M. Hrabalikova, J. Osicka, M. Cvek, M. Sedlacik, B. Hanulikova, L. Munster, D. Skoda, P. Urbánek, J. Pietrasik, J. Mosnacek, Effect of structure of polymers grafted from graphene oxide on the compatibility of particles with a silicone-based environment and the stimuli-responsive capabilities of their composites, Nanomaterials 10 (2020), **https://doi.org/10.3390/ nano10030591**.

[27] Y. Chen, P. Hu, Z. Huang, J. Wang, H. Song, X. Chen, X. Lin, T. Wu, X. Tan, Significant enhancement of the polarization holographic performance of photopolymeric materials by introducing graphene oxide, ACS Appl. Mater. Interfaces 13 (2021) 27500-27512, **https://doi.org/10.1021/acsami.1c07390**.

[28] J. Zhang, M. Zuo, X. Lv, H. Zhang, Q. Zheng, Effect of grafted graphene nanosheets on morphology evolution and conductive behavior of poly(methyl methacrylate)/ poly(styrene-: Co -acrylonitrile) blends during isothermal annealing, RSC Adv. 8 (2018) 14579-14588, **https://doi.org/10.1039/c8ra00439k**.

[29] M. Suess, J. Kressler, H.W. Kammer, The miscibility window of poly (methylmethacrylate)/poly(styrene-co-acrylonitrile) blends, Polymers 28 (1987) 957-960, **https://doi.org/10.1016/0032-3861(87)90169-8**.

[30] M. Sumita, K. Sakata, S. Asai, K. Miyasaka, H. Nakagawa, Dispersion of fillers and the electrical conductivity of polymer blends filled with carbon black, Polym. Bull. 25 (1991) 265-271, **https://doi.org/10.1007/BF00310802**.

[31] S. Ahadian, M. Mohseni, S. Moradian, Ranking proposed models for attaining surface free energy of powders using contact angle measurements, Int. J. Adhes. Adhes. 29 (2009) 458-469, **https://doi.org/10.1016/j.ijadhadh.2008.09.004**.

[32] H.J. Chung, J. Kim, K. Ohno, R.J. Composto, Controlling the location of nanoparticles in polymer blends by tuning the length and end group of polymer brushes, ACS Macro Lett. 1 (2022) 252-256, **https://doi.org/10.1021/mz200068p**.

[33] C.R. López-Barrón, C.W. Macosko, Rheology of compatibilized immiscible blends with droplet-matrix and cocontinuous morphologies during coarsening, J. Rheol. (N. Y. N. Y 58 (2014) 1935-1953, **https://doi.org/10.1122/1.4897409**.

[34] R. Li, W. Yu, C. Zhou, Phase behavior and its viscoelastic responses of poly(methyl methacrylate) and poly(styrene-co-maleic anhydride) blend systems, Polym. Bull. 56 (2006) 455-466, **https://doi.org/10.1007/s00289-005-0499-6**.

[35] P.H.P. Macaubas, N.R. Demarquette, Time-temperature super position principie applicability for blends formed of immiscible polymers, Polym. Eng. Sci. 42 (2002) 1509-1519, **https://doi.org/10.1002/pen.11047**.

[36] C. Gao, P. Liu, Y. Ding, T. Li, F. Wang, J. Chen, S. Zhang, Z. Li, M. Yang, Noncontact percolation of unstable graphene networks in poly(styrene-co-acrylonitrile) nanocomposites: electrical and rheological properties, Compos. Sci. Technol. 155 (2018) 41-49, **https://doi.org/10.1016/j.compscitech.2017.11.023**.

[37] R. Hasegawa, Y. Aoki, M. Doi, Optimum graft density for dispersing particles in polymer melts, Macromolecules 29 (1996) 6656-6662, **https://doi.org/10.1021/ ma960365x**.

[38] S.H. Yang, J.W. Lee, H. Kim, Localization behavior of multiwalled carbon nanotubes in ternary blends of PC, SAN, and PMMA, Korea Aust. Rheol. J. 32 (2020) 145-152, **https://doi.org/10.1007/s13367-020-0013-6**.